Exceptionally Robust $CuInS_2$/ZnS Nanoparticles as Single Component Photocatalysts for H_2 Evolution

Yulu Zhou,[a†] Wenhui Hu,[b†] John Ludwig,[b] Jier Huang[b*]

[a]College of Science, China University of Petroleum (East China), Qingdao, China, 266580.

[b]Department of Chemistry, Marquette University, Milwaukee, Wisconsin, 53201.

Corresponding Author

*Jier Huang (jier.huang@marquette.edu)

ABSTRACT. In this work, we report water soluble $CuInS_2$/ZnS nanoparticles (NPs) as intrinsic single-component photocatlaysts for light-driven hydrogen generation. In the presence of ascorbic acid (AA), this catalyst can efficiently generate H_2 from water with an exceptionally long lifetime (>>84 hours). Mechanistic insight into the catalysis revealed by transient absorption spectroscopy demonstrates that the catalytic cycle initiates by a reductive quenching process through electron transfer from AA to $CuInS_2$/ZnS NPs, which is followed by a rate limiting step, i.e. proton reduction from electrons in the conduction band/defect states of the $CuInS_2$/ZnS NPs.

Introduction

Solar H_2 generation through photocatalytic water splitting, an attractive strategy to partially resolve the energy crisis, requires an efficient photocatalytic system that is not only capable of efficient light harvesting but also that can perform the subsequent catalytic reaction.[1, 2] Since the initial report of light-driven H_2 generation,[3, 4] extensive efforts have been made to develop semiconductor nanocrystals as photocatalytic materials.[5-8] Among the various kinds of semiconductor nanocrystals reported, most of them are either wide band gap semiconductors,[9, 10] which only respond to UV light, or contain highly toxic element, such as Cd and Pb, largely limiting their practical application.[11] As a result, there is significant interest in developing multinary semiconductor nanocrystals to replace these highly toxic materials for photocatalytic applications.

Given their success as cathode materials in photovoltaic devices,[12, 13] Chalcopyrite-type $CuInS_2$ (CIS) nanocrystals and related materials have emerged as one of the most promising alternatives for photocatalytic application because of their easily tunable bandgap that can be controlled by size and chemical composition, high extinction coefficient, and well-positioned conduction band for hydrogen evolution reaction (HER).[14-18] For instance, CIS or its analogues loaded with noble metals[17-19] or MoS_2[20] as cocatalysts have been reported for H_2 generation from water. Very recently, CIS has been successfully used as photocathode materials in overall water splitting cell.[21-23] While these examples evidently demonstrate the promise of CIS nanocrystals in photocatalysis, the role of CIS in these examples are mainly photosensitizers, where the second component, i.e. cocatalysts, are required to boost HER activity. This not only complicates the system design but also leads to the challenge in effective coupling between the photosensitizer and catalyst, a key factor that determines the efficiency of HER. To address these

limitations, herein we report a single-component photocatalytic system, CIS/ZnS nanoparticles (NPs), that can efficiently catalyze HER in aqueous solution with exceptionally long duration. More importantly, using transient absorption spectroscopy, we unraveled the fundamental catalytic mechanism for HER.

Experimental Methods.

Chemicals and Materials. CuI, $In(OAc)_3$, $Zn(OAc)_2$, 1-dodecanethiol (DDT), mercaptopropionic acid (MPA), 1-octadecene (ODE), oleic acid (OA) and oleylamine (OLA) were purchased from Sigma-Aldrich. The rest chemicals and solvents were purchased from VWR. All chemicals were used as received without further purification.

The Synthesis of CIS/ZnS NPs. Water soluble CIS/ZnS NPs capped with mercaptopropionic acid (MPA) were synthesized according to the previously published procedures with minor modification.[24] The CIS NPs were coated with an additional layer of ZnS to improve their photostability and emission quantum yield.[25] In a typical synthesis, CuI (38 mg, 0.2 mmol), $In(OAc)_3$ (232 mg, 0.8 mmol), $Zn(OAc)_2$ (88 mg, 0.5 mmol), 1-dodecanethiol (DDT) (2 mL), and 1-octadecene (ODE) (4 mL) were mixed in a three-necked flask. The reaction mixture was degassed with N_2 for 30 min at room temperature. After that, the mixture was heated to 120°C until a clear yellow solution was formed. 1 mL of oleic acid (OA) was then added into the solution. The mixture was heated to 230°C, after which a deep orange red colloidal solution was formed (~ 15 min), indicating the formation of CIS NPs. For further growth of ZnS shell, Zn stock solution (4 mL) (see below for details) was added dropwise into the reaction mixture immediately. The Zinc stock solution was prepared in advance by mixing $Zn(OAc)_2$ (528 mg, 3 mmol), oleylamine (OLA) (2 mL), and ODE (2 mL) in a flask, which is followed by degassing

with N_2 for 30 min and heated to 130 °C until a colorless solution was formed. The reaction was quenched after cooling the reaction system to room temperature. The resulting CIS/ZnS NPs were isolated by precipitating using acetone, followed by centrifuging and decanting the supernatant.

The Synthesis of Water Soluble CIS/ZnS NPs. The water soluble CIS/ZnS NPs were prepared through ligand exchange procedure in the presence of mercaptopropionic acid (MPA). Briefly, 3 mL of MPA (30 mmol), 200 mg of CIS/ZnS QDs powder and 6 mL of N,N-dimethylformamide (DMF) were added into a flask, and degassed with N_2 for 30 min. Then, the mixture was heated to 130 °C and stirred for 15 min, resulting the formation of = a clear solution. The CIS/ZnS was then precipitated out by adding 35 mL of 2-propanol and centrifugated at 5000 rpm for 5 min. The precipitates (80 mg) were dissolved in 40 mL of alkaline water stock solution (pH ~10, NaOH), the OD was measured to be 3.64 at 400 nm and the fluorescence emission peak was 587 nm (excited with a 420 nm light).

Photochemical Hydrogen Generation. All photocatalytic reactions were performed in a 9 mL vial under the illumination of 405 nm LED (85 mW). In a general process, a certain amount of CIS/ZnS stock solution was mixed with ascorbic acid (AA) (1.00 mL, 0.2 M in H_2O) in a sample vessel. The total volume of the solution was adjusted to 2.0 mL. The vial was sealed, degassed with nitrogen, and transferred to photocatalysis apparatus. The amount of evolved hydrogen was quantified by a Agilent 490 micro gas chromatograph (5 Å molecular sieve column), after taking 200 μL of the headspace of the vial.

Standard Characterization. UV-Visible absorption spectra were taken using an Agilent 8453 spectrometer. Steady state emission spectrum was measured using a PTI QM40. The XRD patterns were performed using a Rigaku Miniflex II XRD diffractometer with Cu Kα radiation.

TEM was taken with a JEOL JEM-2100UHR electron microscope. EDX data were collected on a Hitachi S-4800 Scanning Electron Microscope with an EDAX XM2-60S energy dispersive spectrometer.

Femtosecond Absorption Spectroscopy. The femtosecond absorption spectrometer is based on a regenerative amplified Ti-Sapphire laser system (Solstice, 800nm, < 100 fs FWHM, 3.5 mJ/pulse, 1 KHz repetition rate). The tunable pump is generated in TOPAS which has output with tunable wavelength ranging from 254 nm to 1100 nm. The tunable UV-visible probe pulses are generated by while light generation in a Sapphire window (430-750 nm) on a translation stage. The femtosecond transient absorption is performed in Helios ultrafast spectrometer (Ultrafast Systems LLC). The sample cuvette path length was 2 mm.

Results and Discussion

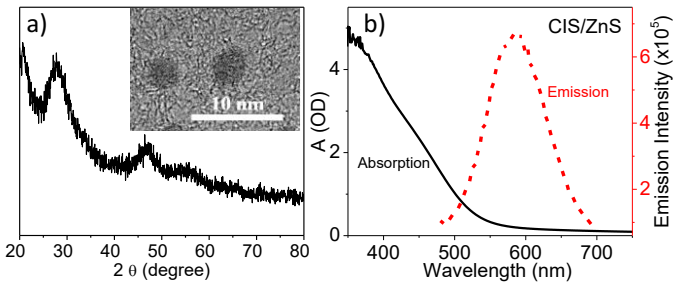

Figure 1. (a) XRD patterns and TEM image (inset) of CIS/ZnS NPs. (b) UV-visible and emission spectrum of CIS/ZnS NPs taken using 2 mg/mL and 0.16 mg/mL NPs in water solution, respectively.

Figure 1a shows the XRD patterns of the as-prepared CIS/ZnS NPs. The three main peaks with 2θ values at 27.8°, 46.9°, and 54.9°, which agree well with the literature data of CIS and CIS/ZnS,[26, 27] support the tetragonal crystal structure. The morphology of the NPs was measured using TEM. As shown in the inset of Figure 1a, the NPs displayed clear lattice fringes with

average size of ~ 3.5 nm in diameter. The chemical composition of Cu, In, and S ratio was examined by energy-dispersive X-ray spectroscopy (EDX). As shown in Figure S1, the atomic percent of Zn in CIS/ZnS NPs (3.65%) increased significantly compared to that in CIS NPs (0.65%), suggesting that ZnS has been coated onto CIS surface successfully. In addition, from the onset of the UV-visible absorption spectrum (Figure 1b), the optical bandgap of CIS/ZnS NPs was estimated to be 2.2 eV, close to the value in previous literature reports.[28, 29] The emission spectrum of the as-synthesized CIS/ZnS NPs is also shown in Figure 1b. The water soluble CIS/ZnS NPs exhibit an emission quantum yield of 6.2% (see supporting information).

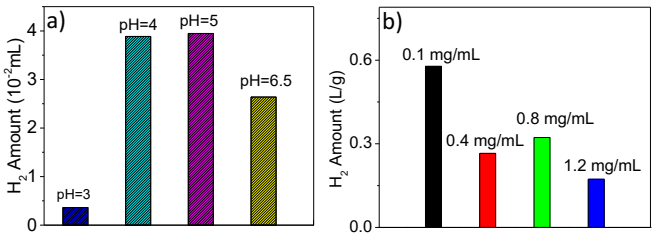

Figure 2. The dependence of H_2 production on pH values of AA (a) and concentration of CIS/ZnS NPs (b). The photocatalytic reactions were performed under 405 nm (85 mW) light illumination in the presence of AA. 0.1 mg/mL CIS/ZnS NPs with 24 hours' collection were used for pH dependence experiments.

Photocatalytic H_2 generation experiments were performed in a custom-designed photocatalytic apparatus, consisting of a DC power supply and a 405 nm LED lamp. A series of photocatalytic experiments were first explored to find the optimum conditions for H_2 generation, as experimental parameters such as pH values and concentrations of photocatalysts can easily affect the efficiency of light-driven H_2 production. Among the varying pH values of AA, the CIS/ZnS NPs system with pH = 5.0 AA gave the highest activity, and was thus identified as most appropriate pH value for the HER reaction (Figure 2a). Next, the HER activity with different

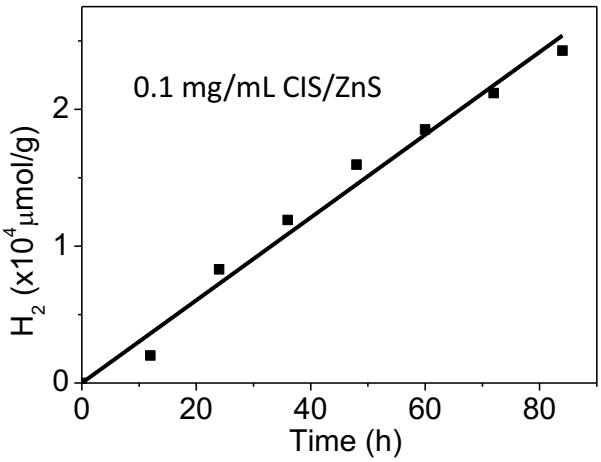

Figure 3. H_2 generation time profile of CIS/ZnS NPs under 405 nm illumination in the presence of AA (pH=5).

concentration of CIS/ZnS NPs was measured. As shown in Figure 2b, the sample with 0.1 mg/mL CIS/ZnS NPs shows the highest HER activity in terms of the volume of H_2/g of NPs, and is thus used as the optimum concentration of NPs. The dependence of H_2 production on pH values and NP concentrations were also performed under 505 nm LED illumination. As the amount of H_2 generated under 505 nm illumination (Figure S3) is much less than that generated under 405 nm, 405 nm LED is then adopted as the optimum light source. Using these conditions, the HER activity of the CIS/ZnS NPs as a function of time was measured under illumination of 405 nm LED lamp. Figure 3 shows the time profile of H_2 production. Remarkably, the CIS/ZnS photocatalytic system remains active for HER over 84 hours. The HER efficiency of CIS/ZnS reached 24.3 mmol H_2/g after 84 h of reaction.

The HER activity of our single-component CIS/ZnS system is noteworthy in comparison with previously reported CIS or CIS based catalysts for HER. It has been shown that CIS based systems with cocatalyst loading can efficiently produce H_2 with HER activity in the range of 10^{-1}-10^2 mmol H_2/g. [17-19, 30, 31] However, in the absence of cocatalyst, they typically do not perform

well as a photocatalyst for HER. To best of our knowledge, systems without cocatalysts typically show HER activity with < 0.1 mmol/g of CIS, [18, 31] except for one example based on CIS/ZnS alloy which produced ~ 21.6 mmol H_2/g of NPs.[32] Note that the HER activity (24.3 mmol/g) in our system is indeed better than that of previously reported best-performing system. The current CIS/ZnS system, however, benefits from significantly longer duration, i.e. >> 84 hours in the current system vs. 22 hours for the above-mentioned CIS/ZnS alloyed system. Unfortunately, both external (~ 0.01%) and internal quantum efficiency (~ 0.03%) for H_2 generation of the current system are << 1% under both 405 nm and 505 nm illumination, suggesting that a cocatalyst is still necessary for future application of CIS/ZnS NPs in HER. Nevertheless, the current work demonstrates the exceptional stability of water soluble CIS/ZnS NPs for photocatalytic application.

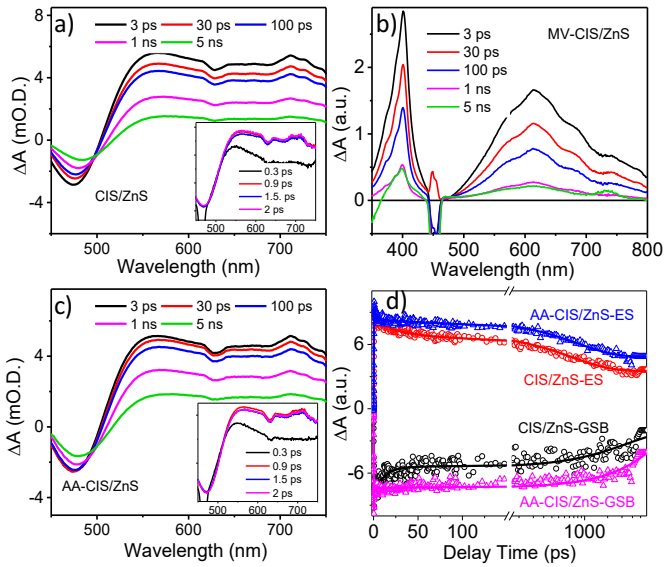

Figure 4. Femtosecond transient absorption spectra of CIS/ZnS NPs (a), in the presence of MV^{2+} (b) and AA (c). The early time spectra of CIS/ZnS in the presence of MV^{2+} are shown in Figure S4. (d) The comparison of kinetic traces of ground state bleach recovery and excited state decay of CIS/ZnS NPs in the absence and presence of AA.

In order to gain insight on catalytic mechanism of the current CIS/ZnS system, femtosecond transient absorption (TA) spectroscopy was used to investigate the light harvesting and charge separation dynamics of CIS/ZnS NPs, the key properties that dictate the function of CIS/ZnS NPs for photocatalysis. Figure 4a shows the TA spectra of CIS/ZnS NPs following 450 nm excitation. There are two main features observed in the TA spectra of CIS/ZnS NPs, including a negative feature centered at 470 nm and a broad positive absorption at >550 nm. The former can be assigned to the ground state bleach (GSB) of CIS/ZnS NPs, which results from the promotion of electrons from the valance band to the conduction band of NPs, leading to the depopulation of valence band electrons. The positive feature, which disappears in the presence of methyl viologen (electron acceptor) and is accompanied by the formation of the reduced state of methyl

viologen[33] (Figure 4b), can be attributed to the electron absorption of the excited state CIS/ZnS NPs. A clear isosbestic point was observed at ~ 500 nm, suggesting that the decay of these two features correspond to the same relaxation process, i.e. the recombination of electrons in the conduction band/electron trap state with the holes in the valence band/ hole trap states. Because the electron-hole recombination time is much longer than the time window of our TA spectroscopy (~ 5 ns), we are not able to accurately determine the electron-hole pair lifetime in CIS/ZnS NPs. Nevertheless, we can use these features as probes to follow the carrier relaxation dynamics in these NPs.

In the presence of AA (pH=5), the TA spectra of CIS/ZnS NPs (Figure 4c) resembles the spectra without AA. However, a slight difference was observed in their kinetic traces (Figure 4d), where the kinetic traces of NPs in the presence of AA show a slightly slower decay than those without AA, in terms of both GSB and electron absorption. As AA is a well-known electron donor, the decreased decay/recovery dynamics in the sample with AA can be attributed to the electron transfer (ET) process from AA to CIS/ZnS NPs, resulting a longer lifetime of electrons in the conduction band/trap states. This explains the observed high HER activity, as the elongated charge separated state, i.e. holes in AA and electrons in CIS/ZnS NPs, effectively inhibited electron/hole recombination and facilitated H_2 generation. On the other hand, these TA results also suggest that the process of ET from the conduction band/trap states of CIS/ZnS NCs to reduce proton cannot compete with ET from AA to the valence band of CIS/ZnS NPs. This is because the removal of electrons in the conduction band of CIS/ZnS NPs is expected to enhance the GSB recovery and electron absorption decay, which conflicts with what we observed in TA measurements. These results together suggest that the catalytic cycle for HER initiates with the reductive quenching process through ET from AA to CIS/ZnS NPs, which is followed by proton

reduction through ET from CIS/ZnS NPs. Because of our limited time window of TA spectroscopy, we are not able to accurately determine the ET rate from TA kinetics. Instead, we estimated the ET rate constant through measuring steady state emission quenching as a function of AA concentration. By modeling the emission intensity/AA concentration plot through Stern-Volmer equation (Figure S5), we obtained the ET rate constant with 1.15×10^8 M^{-1} S^{-1}.

In summary, we have reported an exceptionally robust single-component CIS/ZnS NPs photocatalyst for HER in aqueous solution. This photocatalyst does not show degradation even after 84 hours of illumination. To best of our knowledge, this represents the most robust CIS based photocatalytic system for light-driven production of H_2. Furthermore, the HER activity of the current CIS/ZnS system shows 24.3 mmol/g NPs, which compares well with the best performing system reported previously. Such high efficiency can be attributed to effective charge separation through ET from AA to CIS/ZnS NPs, which elongated the lifetime of the electrons in the NPs and ultimately facilitate proton reduction to generate H_2. The catalytic cycle was found to initiate with reductive quenching process of CIS/ZnS NPs, suggesting that proton reduction process is the rate determining process for HER. These results suggest the great potential of CIS/ZnS NPs as robust and non-toxic photocatalysts for solar fuel conversion.

ASSOCIATED CONTENT

Supporting Information. EDX analysis, quantum yield measurement, H_2 generation under 505 nm illumination, early time TA spectra of CIS/ZnS NPs in the presence of MV^{2+}, emission quenching experiment by AA, Stern-Volmer modeling are available free of charge via the Internet at http://pubs.acs.org."

AUTHOR INFORMATION

Corresponding Author

jier.huang@marquette.edu

†These authors are equally attributed to the work.

Notes

The authors declare no competing financial interests.

ACKNOWLEDGMENT

This work was supported by National Science Foundation (DMR-1654140).

REFERENCES

(1). Gratzel, M., Artificial Photosynthesis - Water Cleavage into Hydrogen and Oxygen by Visible-Light. Acc. Chem. Res. 1981, 14, 376-384.

(2). Chen, X. B.; Shen, S. H.; Guo, L. J.; Mao, S. S., Semiconductor-Based Photocatalytic Hydrogen Generation. Chem. Rev. 2010, 110, 6503-6570.

(3). Fujishima, A.; Honda, K., Electrochemical Photolysis of Water at a Semiconductor Electrode. Nature 1972, 238, 37.

(4). Lehn, J. M.; Sauvage, J. P., Chemical Storage of Light Energy - Catalytic Generation of Hydrogen by Visible-Light or Sunlight - Irradiation of Neutral Aqueous-Solutions. Nouv. J. Chim. 1977, 1, 449-451.

(5). Han, Z. J.; Qiu, F.; Eisenberg, R.; Holland, P. L.; Krauss, T. D., Robust Photogeneration of H-2 in Water Using Semiconductor Nanocrystals and a Nickel Catalyst. Science 2012, 338, 1321-1324.

(6). Qiu, F.; Han, Z. J.; Peterson, J. J.; Odoi, M. Y.; Sowers, K. L.; Krauss, T. D., Photocatalytic Hydrogen Generation by Cdse/Cds Nanoparticles. Nano Lett. 2016, 16, 5347-5352.

(7). Wu, K. F.; Zhu, H. M.; Liu, Z.; Rodriguez-Cordoba, W.; Lian, T. Q., Ultrafast Charge Separation and Long-Lived Charge Separated State in Photocatalytic Cds-Pt Nanorod Heterostructures. J. Am. Chem. Soc. 2012, 134, 10337-10340.

(8). Huang, J.; Mulfort, K. L.; Du, P. W.; Chen, L. X., Photodriven Charge Separation Dynamics in Cdse/Zns Core/Shell Quantum Dot/Cobaloxime Hybrid for Efficient Hydrogen Production. J. Am. Chem. Soc. 2012, 134, 16472-16475.

(9). Sasan, K.; Lin, Q.; Mao, C.; Feng, P., Incorporation of Iron Hydrogenase Active Sites into a Highly Stable Metal-Organic Framework for Photocatalytic Hydrogen Generation. Chem. Commun. 2014, 50, 10390-10393.

(10). Yu, J. G.; Qi, L. F.; Jaroniec, M., Hydrogen Production by Photocatalytic Water Splitting over Pt/Tio2 Nanosheets with Exposed (001) Facets. J. Phys. Chem. C 2010, 114, 13118-13125.

(11). Hardman, R., A Toxicologic Review of Quantum Dots: Toxicity Depends on Physicochemical and Environmental Factors. Environ. Health Persp. 2006, 114, 165-172.

(12). Romanyuk, Y. E.; Hagendorfer, H.; Stucheli, P.; Fuchs, P.; Uhl, A. R.; Sutter-Fella, C. M.; Werner, M.; Haass, S.; Stuckelberger, J.; Broussillou, C. et al. All Solution-Processed

Chalcogenide Solar Cells - from Single Functional Layers Towards a 13.8% Efficient Cigs Device. Adv Funct Mater 2015, 25, 12-27.

(13). Chirila, A.; Reinhard, P.; Pianezzi, F.; Bloesch, P.; Uhl, A. R.; Fella, C.; Kranz, L.; Keller, D.; Gretener, C.; Hagendorfer, H. et al. Potassium-Induced Surface Modification of $Cu(in,Ga)Se_2$ Thin Films for High-Efficiency Solar Cells. Naure Mater. 2013, 12, 1107-1111.

(14). Zhang, L.; Minegishi, T.; Nakabayashi, M.; Suzuki, Y.; Seki, K.; Shibata, N.; Kubota, J.; Domen, K., Durable Hydrogen Evolution from Water Driven by Sunlight Using $(Ag,Cu)GaSe_2$ Photocathodes Modified with CdS and $CuGa_3Se_5$. Chem. Sci. 2015, 6, 894-901.

(15). Kumagai, H.; Minegishi, T.; Moriya, Y.; Kubota, J.; Domen, K., Photoelectrochennical Hydrogen Evolution from Water Using Copper Gallium Selenide Electrodes Prepared by a Particle Transfer Method. J. Phys. Chem. C 2014, 118, 16386-16392.

(16). Guijarro, N.; Prevot, M. S.; Yu, X. Y.; Jeanbourquin, X. A.; Bornoz, P.; Bouree, W.; Johnson, M.; Le Formal, F.; Sivula, K., A Bottom-up Approach toward All-Solution-Processed High-Efficiency $Cu(in,Ga)S_2$ Photocathodes for Solar Water Splitting. Adv. Energy Mater. 2016, 6.

(17). Tsuji, I.; Kato, H.; Kudo, A., Visible-Light-Induced H_2 Evolution from an Aqueous Solution Containing Sulfide and Sulfite over a $ZnS-CuInS_2-AgInS_2$ Solid-Solution Photocatalyst. Angew. Chem., Int. Edit. 2005, 44, 3565-3568.

(18). Tsuji, I.; Kato, H.; Kobayashi, H.; Kudo, A., Photocatalytic H_2 Evolution under Visible-Light Irradiation over Band-Structure-Controlled $(CuIn)_XZn_{2(1-X)}S_2$ Solid Solutions. J. Phys. Chem. B 2005, 109, 7323-7329.

(19). Zheng, L.; Xu, Y.; Song, Y.; Wu, C. Z.; Zhang, M.; Xie, Y., Nearly Monodisperse $CuInS_2$ Hierarchical Microarchitectures for Photocatalytic H_2 Evolution under Visible Light. Inorg. Chem. 2009, 48, 4003-4009.

(20). Yuan, Y. J.; Chen, D. Q.; Huang, Y. W.; Yu, Z. T.; Zhong, J. S.; Chen, T. T.; Tu, W. G.; Guan, Z. J.; Cao, D. P.; Zou, Z. G., MoS_2 Nanosheet-Modified $CuInS_2$ Photocatalyst for Visible Light-Driven Hydrogen Production from Water. Chemsuschem 2016, 9, 1003-1009.

(21). Iwase, A.; Yoshino, S.; Takayama, T.; Ng, Y. H.; Amal, R.; Kudo, A. Water Splitting and CO_2 Reduction under Visible Light Irradiation Using Z-Scheme Systems Consisting of Metal Sulfides, CoOx-Loaded $BiVO_4$, and a Reduced Graphene Oxide Electron Mediator. J. Am. Chem. Soc. 2016, 138, 10260-10264.

(22). Iwashina, K.; Iwase, A.; Ng, Y. H.; Amal, R.; Kudo, A., Z-Schematic Water Splitting into H_2 and O_2 Using Metal Sulfide as a Hydrogen-Evolving Photocatalyst and Reduced Graphene Oxide as a Solid-State Electron Mediator. J. Am. Chem. Soc. 2015, 137, 604-607.

(23). Kaneko, H.; Minegishi, T.; Nakabayashi, M.; Shibata, N.; Kuang, Y. B.; Yamada, T.; Domen, K., A Novel Photocathode Material for Sunlight-Driven Overall Water Splitting: Solid Solution of Znse and $Cu(in,Ga)Se_2$. Adv. Funct. Mater. 2016, 26, 4570-4577.

(24). Zhao, C. Z.; Bai, Z. L.; Liu, X. Y.; Zhang, Y. J.; Zou, B. S.; Zhong, H. Z., Small GSH-Capped $CuInS_2$ Quantum Dots: Mpa-Assisted Aqueous Phase Transfer and Bioimaging Applications. ACS Appl. Mater. Inter. 2015, 7, 17623-17629.

(25). Bux, H.; Feldhoff, A.; Cravillon, J.; Wiebcke, M.; Li, Y.-S.; Caro, J., Oriented Zeolitic Imidazolate Framework-8 Membrane with Sharp H_2/C_3h_8 Molecular Sieve Separation. Chem. Mater. 2011, 23, 2262-2269.

(26). Xiong, W. W.; Yang, G. H.; Wu, X. C.; Zhu, J. J., Aqueous Synthesis of Color-Tunable $CuInS_2$/ZnS Nanocrystals for the Detection of Human Interleukin 6. ACS Appl. Mater. Inter. 2013, 5, 8210-8216.

(27). Chen, Y. Y.; Li, S. J.; Huang, L. J.; Pan, D. C., Green and Facile Synthesis of Water-Soluble Cu-In-S/ZnS Core/Shell Quantum Dots. Inorg. Chem. 2013, 52, 7819-7821.

(28). Panthani, M. G.; Akhavan, V.; Goodfellow, B.; Schmidtke, J. P.; Dunn, L.; Dodabalapur, A.; Barbara, P. F.; Korgel, B. A., Synthesis of $CuInS_2$, $CuInSe_2$, and $Cu(In_xGa_{1-X})Se_2$ (CiGS) Nanocrystal "Inks" for Printable Photovoltaics. J. Am Chem. Soc. 2008, 130, 16770-16777.

(29). Wang, X. L.; Pan, D. C.; Weng, D.; Low, C. Y.; Rice, L.; Han, J. Y.; Lu, Y. F., A General Synthesis of Cu-In-S Based Multicomponent Solid-Solution Nanocrystals with Tunable Band Gap, Size, and Structure. J. Phys. Chem. C 2010, 114, 17293-17297.

(30). Ye , C.; Regulacio, M. D.; Lim, S. H.; Li, S.; Xu, Q. H.; Han, M. Y., Alloyed ZnS-$CuInS_2$ Semiconductor Nanorods and Their Nanoscale Heterostructures for Visible-Light-Driven Photocatalytic Hydrogen Generation. Chemistry-a European Journal 2015, 21, 9514-9519.

(31). Zhang, X. H.; Du, Y. C.; Zhou, Z. H.; Guo, L. J., A Simplified Method for Synthesis of Band-Structure-Controlled $(CuIn)_XZn_{2(1-X)}S_2$ Solid Solution Photocatalysts with High Activity of Photocatalytic H_2 Evolution under Visible-Light Irradiation. Int. J. Hydrogen Energ. 2010, 35, 3313-3321.

(32). Xu, M.; Zai, J. T.; Yuan, Y. P.; Qian, X. F., Band Gap-Tunable $(CuIn)_XZn_{2(1-X)}S_2$ Solid Solutions: Preparation and Efficient Photocatalytic Hydrogen Production from Water under Visible Light without Noble Metals. J. Mater. Chem. 2012, 22, 23929-23934.

(33). Peon, J.; Tan, X.; Hoerner, J. D.; Xia, C. G.; Luk, Y. F.; Kohler, B., Excited State Dynamics of Methyl Viologen. Ultrafast Photoreduction in Methanol and Fluorescence in Acetonitrile. J. Phys. Chem. A 2001, 105, 5768-5777.

TOC Graphic